Enhancement of the Absolute Negative Mobility effect in geometrically improved microfluidic devices

Sébastian Grauwin

18 septembre 2006

Résumé

As the application in microbiology go down in size, the influence of the thermal noise (Brownian motion) is less and less negligeable and can even be used in determined purposes. In especially designed microstructured channels made of poly(dimethylsiloxane) (PDMS), the interplay of thermal noise and an alternating force is at the origin of a counter-intuitive motion of particles moving on average in a direction opposite to that of the applied force. This phenomenon (Absolute Negative Mobility, or ANM) had been theoretically predicted and already observed with success. The aims of the work presented here was to test new geometrically modified microstructured channels. We observe ANM responses up to 9 times higher than in the previous structures, in excellent agreement with the simulations. We also discovered and characterized in one of the modified channels a new and unexpected hybrid mechanism which mix features of the first ANM mechanism with those of a normal deterministic mechanism.

keywords : Microfluidic devices, diffusion, Absolute Negative Mobility, PDMS, geometric traps.

University of Bielefeld, Department of Biophysics, Experimental Biophysics & Applied Nanosciences
Bielefeld University, Physics Faculty

Jan Regtmeier
Alexandra Ros

1 Introduction : basic description of ANM

In the early nineties, the apparition of the "micro total chemical analysis system" concept introduced fluids in the microsystem world. Since then, much effort have been made in order to create microfluidic devices which could integrate all the functions of a macroscopic laboratory on small surfaces. Today, we are able to build "labs-on-a-chip" (basically $2D$ or $3D$ networks of structured micro-channels made out of glass, silicon, or more often polymers) of some square centimeters that can handle, mix, filter, separate or detect molecules. The range of possible applications of these devices is very large. Highly used for the analysis of biological sample (blood, for example), they are in this domain less expensive, less polluting, but above all faster and more efficient than their macroscopic counterparts. They make it possible to analyse quantitatively the chemical contents of a single cell, which can not be done with the use of macroscopic instruments.

All these specificities of the microchips which the biomedical world is benefiting from are the consequence of the scale we are dealing with : the height of the microchannels is typically 1 to $100\,\mu m$. It implies a specific kind of physical behaviour of the fluids. "Microfluidic" deals with fluids of law Reynolds number and thus laminar flows, it deals with a non-negligible influence of charged walls inducing electroosmotic flow, and above all it deals with an important influence of diffusion. At this scale, diffusion is no more a negligible noise but is used as a tool, for example to mix molecules of different species. Diffusion is also one of the crucial components which are at the basis of the effect we will study in this repport.

Considering Newton's second law of dynamic, it seems obvious that a system at rest, when perturbed by an external static force, responds by moving in the direction of that force. Indeed, if the unperturbed system is at thermal equilibrium, any other kind of behaviour (such as a constant motion without external force or a motion in the direction opposite to that of the applied force), is forbidden by the second law of thermodynamics[1]. However, far from equilibrium, no basic principle *a priori* prohibits such counter-intuitive effects. Fig 1 presents the basic idea at the heart of one of those "abnormal" effects : *Absolute Negative Mobility*, or, briefly, ANM.

We are in presence of ANM when upon application of an external static load force F of whatever direction the system responds with an average motion (or current) which runs into the opposite direction . Especially, no average current arises when $F = 0$. The most prominent feature of ANM is then a current-load curves exhibiting a passage through the origin with a negative slope.

ANM has been investigated in different quantum mechanical non-equilibrium systems [1,2] and in models of interacting Brownian particles [3]. The experiments that are presented here are based on recent theoretical work predicting the existence of ANM in classical, single-particle systems [4,5].

In order to observe ANM in a lab-on-a chip, the idea is to create a microfluidic device consisting of periodically arranged posts with alternating small and large gaps. The device is filled with negatively charged beads in an aqueous buffer. Electric fields are

[1]Such responses could be exploited to extract work from a single heat bath, *ie* to create the impossible : a *perpetuum mobile* !

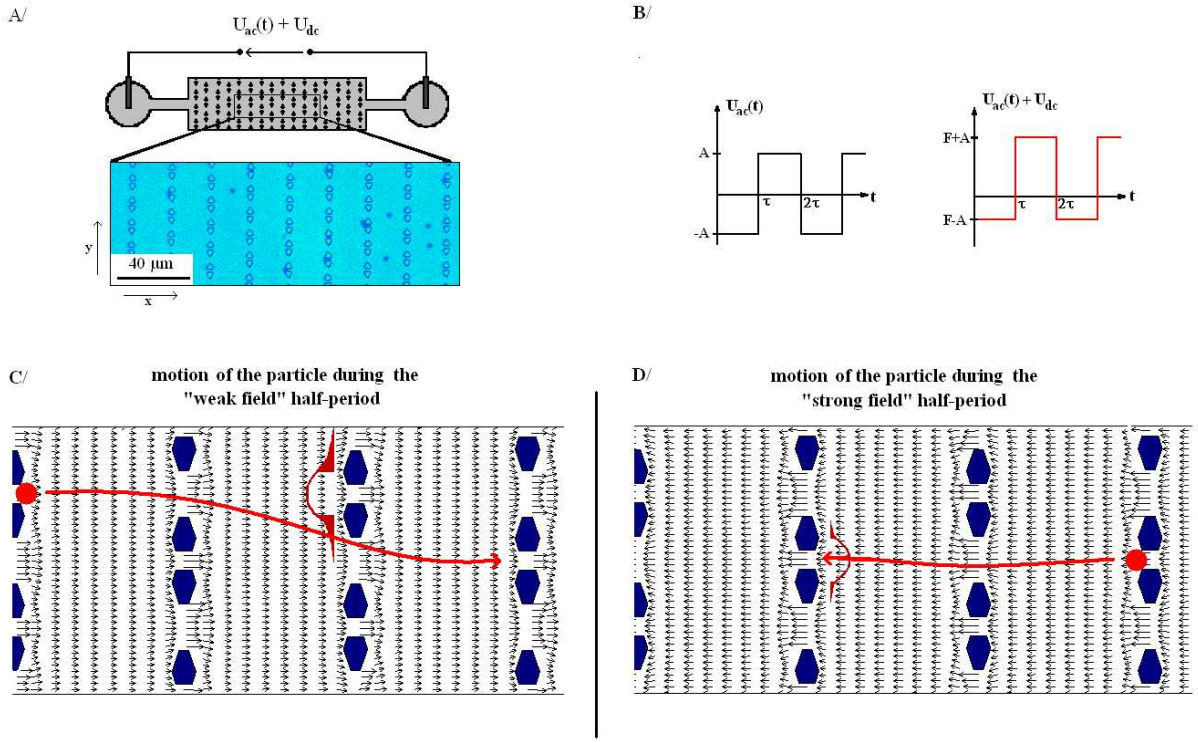

FIG. 1 – A/ Schematic top view of the experimental setup. Electrodes are immersed in the reservoirs of $2mm$ diameter. These reservoirs are connected by narrow channels (length $2500\mu m$ and cross section $24\mu m \times 9\mu m$) to the central microstructured channel (length $6000\mu m$, cross section $400\mu m \times 9\mu m$). The enlargement, an optical micrograph image, shows the periodically arranged posts, together with $2,9\mu m$ diameter carboxylated polystyrene microbeads that are electrokinetically driven by the applied voltage. In each row, the posts have been built in such a way that small gaps through which the beads can not pass alternate with larger ones through which they can. B/ The applied voltage is the sum of an alternative tension U_{AC} that switch periodically between the values $\pm A$ and of an offset voltage $U_{DC} = F$. The U_{AC} voltage keeps the system far from thermal equilibrium and, thanks to the traps formed by the microstructure, produces a unbiased non-linear bead-dynamic. The surimposition of the U_{DC} voltage then breaks the directional symmetry along the x-axis. In ideal condition, we would like the beads to act like this : C/ during the half-period corresponding to the weak voltage ($U = F - A$) the motion along the x-axis is so slow that the beads have enough time to diffuse along the y-axis, thus allowing them to avoid some traps. D/ when switching to the high voltage in the other direction ($U = F - A$), the beads move faster along the x-axis and there is not enough time for them to diffuse before they get caught in the first trap it encounters. During one period, the bead has had an effective motion towards the right side of the channel, whereas the average force is directed towards the left side. The gaussian curves in C/ and D/ give an idea of the proportion of beads that get caught in the traps and the proportion of beads that avoid them.

generated by applying a voltage along the x-axis, so that a positive voltage generates positive force on the beads along the x-axis. We first apply an AC voltage switching periodically between $\pm A$. Due to the symmetry of the AC-drive and of the microstructure, no preferential direction of net motion for the microbead exists. This setup represents an unperturbed non-equilibrium system at rest. The observable of foremost interest is then the average migration velocity in the x-direction $v := < lim_{t\to\infty} \frac{x(t)-x(0)}{t} >$ in response to a static perturbation $U_{DC} = F$ superimposed on the AC voltage. When the parameters A and τ (respectively the modulus and the half-period of the U_{AC} tension) are well chosen, migration velocities which signs are opposite to the corresponding U_{DC} forces can be observed for a whole interval of F values.

In section 2 we present some theoretical facts that are needed to appreciate the physics of microfluids. We also explain how the motion of the beads in the microchannels is simulated and we briefly present the results obtained in the first generation of chips (fig2) to explain why it was interesting to modify the geometry of the posts to enhance the ANM response. The section 3 is devoted to the experimental methods : how we designed and built the chips, how we measured and analyse the motion of the beads. In section 4, we present the results that we obtain with the new chips. Finally, in section 5, we discuss these results. In particular, we oppose two kinds of mechanisms which existed in two slightly different microstructures which both lead on average to an ANM response.

2 Theory

2.1 Microfluidics - generalities

The Reynolds number is defined as $R_e = \frac{L<v>\rho}{\mu}$ where L is the most relevant length scale, μ the viscosity, ρ the fluid density, and $< v >$ the average velocity of the flow. Due to the small dimensions of microchannels, R_e is usually much less than 100, often less than 1. In this Reynolds number regime, flow is completely laminar and no turbulence occurs[2]. Laminar flow provides a means by which molecules can be transported in a relatively predictable manner through microchannels.

There are two common methods by which fluid actuation through microchannels can be achieved. The first one is pressure driven flow, in which the fluid is pumped for instance through syringe pumps. Pressure driven flow can be a relative inexpensive and quite reproducible approach to pumping fluids through microdevices. Another common technique for pumping fluids is that of electroosmotic pumping. If the walls of a microchannel have an electric charge, an electric double layer of counter ions (the "Debye layer") will form along the walls. When an electric field is applied across the channel, the ions in the double layer move towards the electrode of opposite polarity. This creates motion of the fluid near the walls, a motion which gets transmitted to the rest of the fluid by friction. This motion is often refered to as the "EOF", for Electro-Osmotic Flow. One significant disadvantage of EOF is the variability of the channel's surface properties. Proteins or ions, for example, can adsorb to the walls, substantially change

[2]The transition to turbulent flow generally occurs in the range of Reynolds number 2000

the surface charge characteristics and, thereby, change the fluid velocity. This can result in unpredictable long-term time dependencies in the fluid flow.

However, in our experiment, we do not aim at actuating fluid, but only the microbeads it contains. Unfortunately, the electric voltages which induce the electrophoretic motion of the beads also induce electroosmotic motion of the fluid. To reduce this problem, we used a highly concentrated ionic buffer. The length of the Debye layer is given by $\lambda_D = \sqrt{\frac{\epsilon k_B T}{2N_A e^2 I}}$, where $I = \frac{1}{2}\sum c_i {z_i}^2$ is the ionic strength of the buffer, proportionnal to the ions concentrations c_i and the square of their corresponding charges z_i. Higher ionic concentration implies thiner Debye layer, and thus less EOF. With the ion concentration we used, the Debye layer was typically about some nanometer thick.

2.2 Simulation

The motion of a particle in the microstructure is modeled [4,5] by the coupled two-dimensinal overdamped[3] Langevin equation :

$$\gamma\dot{x}(t) = -\partial_x V(x(t), y(t)) + qE_x^*(x(t), y(t))\frac{U_{AC}(t) + U_{DC}}{U^*} + \xi_x(t)$$

$$\gamma\dot{y}(t) = -\partial_y V(x(t), y(t)) + qE_y^*(x(t), y(t))\frac{U_{AC}(t) + U_{DC}}{U^*} + \xi_y(t)$$

where γ denotes the viscouous friction coefficient, $q\vec{E}^*(x, y)$ the effective force on the bead generated by a constant reference voltage $U^* = 1V$ applied to the electrodes, and $V(x, y)$ the effective hard-wall potential generated by the microstuctures (which incorporates the finite radius of the particle). The thermal fluctuations are modeled by the functions $\xi_\alpha(t)$, $\alpha \in \{x, y\}$ which are independent, unbiased Gausian white noises satisfying the fluctuation dissipation relation $< \xi_\alpha(t) * \xi_\alpha(t') >= 2\gamma k_B T\delta(t - t')$, with Boltzmann's constant k_B and room temperature $T \simeq 290K$.

The values of q and γ depends both on the electrophoretic flow and electroosmotic flow (induced in part by the ion cloud surrunding the bead and in part by the channel's walls and posts), but also on the specific conditions prevailing in each chip (geometry, chemical properties of PDMS surface, etc...). Therefore the model is adapted to each given experimental situation. Indeed, the diffusion coefficient D and the mobility μ of the beads can be measured, and thanks to the relations

$$D = \frac{k_B T}{\gamma}$$

$$\mu = \frac{q}{\gamma}$$

we can reach the effective[4] values of q and γ. In practice, only the mobility of the beads has been measured each time, as the diffusion constant of the beads was found to be

[3] $R_e \ll 1$: the inertial forces are negligible before the viscous forces.

[4] effective in the sense that q includes the electrophoretic and electroosmotic forces

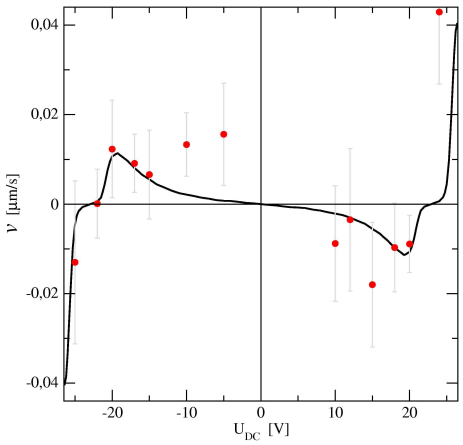

FIG. 2 – Absolute negative mobility of $2\mu m$ beads in the first device, containing rectangular posts. For the AC voltage, an amplitude $A = 30V$ and a switching time $\tau = 25s$ were used. The solid curve represents the theoretical response obtained from the simulations and the dots with error bars correspond to the experimental observation. The way these data are taken and the general shape of the response curve will be explained in the next sections. Note that the highest velocity in the ANM direction is about $0.01\mu m/s$.

rather independant of the small unavoidable changes between the different chips.

At last, the electric field $\vec{E}^*$ is computed by solving the Laplace equation. We used Neumann boundary condition at the borders between the microstructures and the buffer, assuming that the microstructures were perfect insulators, and that the buffer solution was a perfect conductor. Typical results for the electric field are illustrated by the arrows in fig 1 and 3.

2.3 Geometry

It seems obvious that the geometry of the posts, as well as the way they are placed has a major influence on the response of the chips. For example the fact that the posts are symmetrical about the y-axis is directly linked to the fact that there is no average motion of the beads for $U_{DC} = 0$. If the posts presented an asymmetry, there would be a preferential direction, and thus an effective motion at $U_{DC} = 0$ (ratchet effect).

The first experiments[6] were conducted with $3.1\mu m \times 6.1\mu m$ rectangular posts placed in parallel rows $22.5 \pm 0.1\mu m$ apart from each other. In each row, the posts were separated by alternating small gaps of $1.7 \pm 0.1\mu m$ and large gaps of $3.1 \pm 0.1\mu m$.

The electric field $\vec{E}^*$ created by the rectangular posts is represented in fig3-A. The most important feature to observe is the way the electric lines separate just before the posts into lines leading to the small gaps nearby and lines leading to the large ones. It is in fact rather hard to see where the separation occurs, for the arrows just in front of the middle of the rectangles are almost perpendicular to them. Thus, not only did the small gaps act as beads-traps but also did part of the rectangles' ridges, against which the beads are pushed. The separation between the "free zones" centered on the large

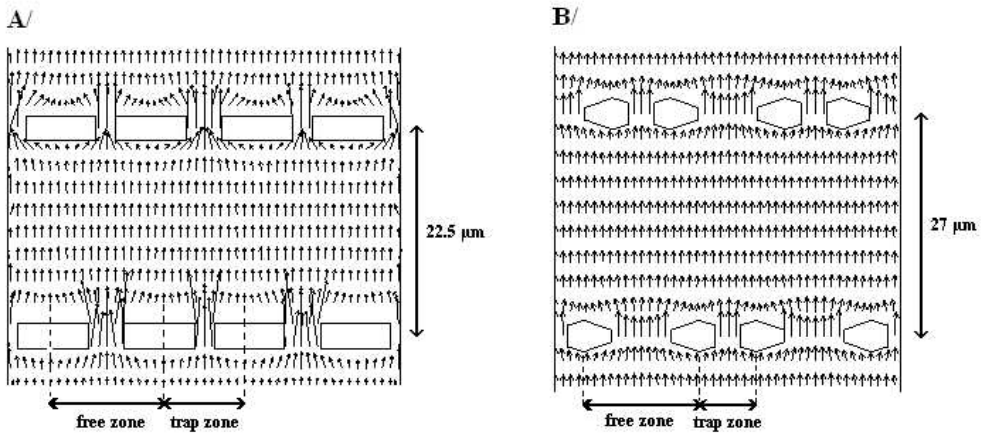

FIG. 3 – Electric field lines computed with the assumptions presented in section 2.2. A/For the first kind of chips containing rectangular posts. B/ For one of the new modified chips containing "triangular" posts. These two figures are not exactly at scale : the rows of rectangles in A/ are $22.5\mu m$ apart whereas the "triangle" rows in B/ are $27\mu m$ apart.

gaps and the "trap zones" centered on the small gaps is therefore not very clear.

The idea which was proposed at this step was to design new chips with geometrically improved posts. The new geometry had to produce a sharper separation of the field lines in order to counteract the effect of the ridge sticking and to have a better control of the beads. Preliminary simulations with square and diamond shaped posts looked promising. Fig3-B shows the electric field lines computed for a chip containing posts with a truncated diamond shape[5]. This is the shape of the main chips we built and worked with.

3 Experimental methods

3.1 Fabrication of the chips

The chips were built in Poly(dimethylsiloxane), or PDMS. PDMS is a widely used silicon-based organic polymer, which has the property to be optically clear and gas permeable. It is also rather inexpensive and easy to use. The fabrication process for one PDMS chip can be subdivided into four main steps : SU-8 mold fabrication and preparation, PDMS casting and curing, fluidic port coring and channel sealing with PDMS slab. The preparation of the SU-8 mold took about 2 hours and, thanks to a careful utilization, it has been used more than 25 times and is still usable. The rest of the fabrication process took each time approximately 6 hours to be completed.

[5]The fabrication process is not precise enough to design real diamond shaped posts. In the following, these posts will be referred to as the "triangular" ones, because when they were first observed through an optical microscope, they gave the impression to have a triangular shape.

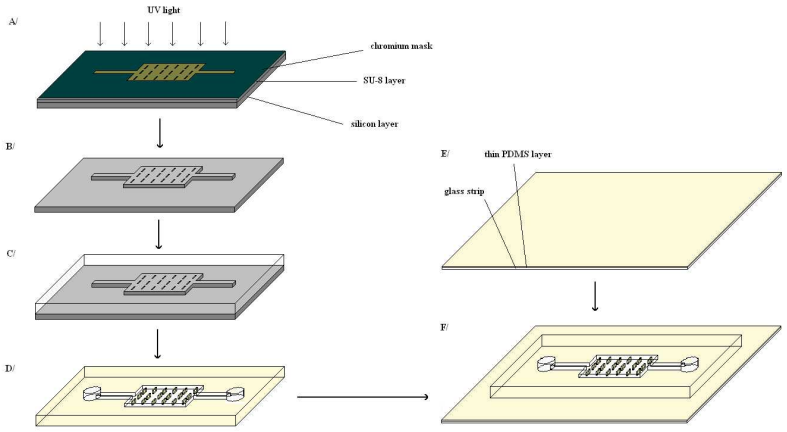

FIG. 4 – A/ A layer of photo resist SU-8 is spin coated on the silicon wafer and then exposed to UV light through a chromium mask. After development we obtain in B/ a structured master wafer that can be used several times. C/ A mixture of the PDMS is poured over the wafer and cured during $4h$ at a temperature of $85\,°C$ D/ The cross-linked PDMS is then easily peeled off the wafer, and two reservoir holes for fluid access are punched at the exterior sides of the narrow channels. E/ Meanwhile, an unstructured PDMS slab has been prepared by pouring, spin coating and curing $30\,min$ at $85\,°C$ another PDMS mixture over a glass slide. F/ Finally, after being exposed to an oxygen plasma the PDMS channel and the unstructured slab are pressed together.

The master wafer is constituted by a silicon layer upon which a negative microstructured layer of SU-8 is created. SU-8 is an epoxy based photoresist and is widely used to create microstructured mold. It is first cast on the silicon wafer and spin coated in order to create a thick SU-8 layer of about $10\mu m$. It is then soft baked (at $60\,°C$ for 5 min), expose to a UV light $(365nm)$ throught an chromium mask, and finally post exposure baked for 20 min at $90\,°C$ to complete the crosslinking of the exposed photoresist (see fig 4-A). The wafer was finally developed by immersion in an diacetone bath, washed with acetone and isopropanol and dried with a nitrogen spray. The final wafer is shown on the photography fig 5. It has roughtly the shape of a disc with a diameter of $13cm$ and it contains as much as 32 structured mold of microchannels.

Once the mold was ready, it could be used to create the real microstructured chips. The first step consisted in preparing $17mL$ of PDMS by mixing the base resin and its curing agent (Sylgard 184 Silicone Elastomer Base and Curing Agent) in a $10:1$ volume ratio. This prepolymer mixture was poured over the wafer and allowed to settle evenly. Once all air bubbles present in the mixture and trapped in the microstructures of the molds had been evacuated (we either left the preparation exuded its air by itself during half an hour or placed the wafer in an excitator and create vacuum during $20\,min$, but without observing any difference between the two methods), the wafer was placed in an oven to cure at $85\,°C$ for 4 hours.

Immediately after the cure was complete, the casting was peeled from the mold and

reservoir holes of a diameter of $2mm$ were punched at the extremities of the channels we wanted to work with. One objective of an optical microscope had been replaced by the punching device on its objective turret. After having spotted one channel extremity with a normal objective, the turret was turned to place the puncher above the chip, then lowered until the punching was done. This method of punching has the advantage to be quite precise and reproducible. The PDMS slab was then cut to retrieve only the microchannels we wanted to work with and placed in a sealed petri box. All these manipulations were realised in a clean room with a controlled atmosphere to prevent the microstructures to be contaminated with dust.

In the meantime, several unstructured PDMS slabs had been prepared by pouring, spin coating and curing $30\,min$ at $85\,°C$ another $10:1$ PDMS mixture over glass slides. The structured surface of the channels and the unstructured PDMS slabs were then put on a grounded aluminium plate in a vacuum chamber. The chamber was evacuated to a pressure of $4 \times 10^{-3}\,mbar$. After taht, an oxygen atmosphere of $0.1\,mbar$ was created. A glow discharge was provided by a charged second parallel electrode placed above the first one. The discharge was run during $30\,s$ and created an oxygen plasma which formed a thin silicon dioxyde layer on the PDMS surfaces. Within seconds of removal from the chamber, the oxidized PDMS surfaces were aligned and pressed together, sealing the channels by chemical bondage. To ensure that the slabs sealed completely, they were left at room temperature for two hours. The oxygen plasma, in addition to ensuring a strong sealing by chemical bondage also renders the PDMS surface of the channel hydrophilic.

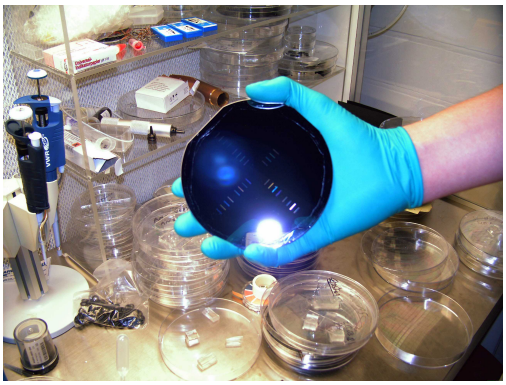

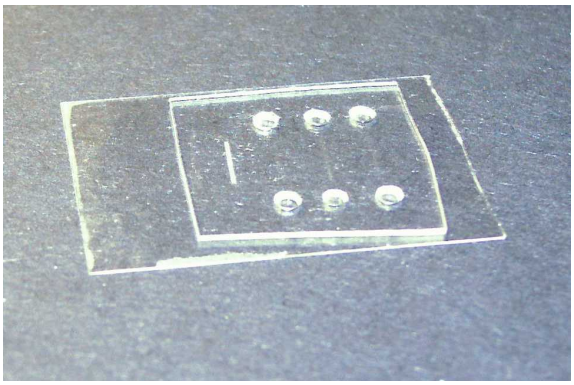

FIG. 5 – Left : the master wafer, where the moulds of 32 channels are divided in 8 different groups of 4 channels. Less than 1/4 of the moulds over this wafer are well enough formed to be used (see section 5.4). Right : a chip containing 4 channels. For three of them, reservoir holes have been punched before assembling the PDMS layer over the glass layer. Here, these three channel are filled with an aqueous solution containing beads, which implies the difference of light refraction between these three channels and the fourth one on the left.

3.2 Beads and buffers

After the two hours period following the chips' assembly, the microchannels were filled with aqueous solution containing $F108$, a derivative of poly(oxyethylene) which adsorbs to the PDMS surface (our "$F108$ solution" was composed of 500 μM of $F108$ dissolved in a $100mM$ phosphate buffer of pH 8.3). This surface treatment inhibits microsphere adsorption and reduces electroosmotic flow [7]. $20mL$ of $F108$ were introduced in one of the reservoir holes with a micropipette, and thanks to the oxygen plasma treatment, it easily filled the microchannels by capillarity. In order to prevent the occurrence of air bubbles within the channels, some of the $F108$ was sucked with a water pump from the channels to the other reservoir holes which were then also filled with $20mL$ of the solution.

Typically, the coated chips were left during around 17 hours on a small support in a petri box containing water. The atmosphere of the petri box loaded by vapor prevented the evaporation of the coating solution. After these 17 hours, the $F108$ was sucked out of the channels.

The solution containing the beads was a $100\,mM$ phosphate buffer of pH 8.3 containing $200\mu M$ of Tween (Tween is the commercial name of polyethylene glycol sorbitan monolaurate, a molecule which renders the aqueous solution viscous). Several kind of beads, of different sizes or surface properties have been tried. However, the results presented in the following sections have all been obtained with the same kind of beads, which size, mobility and diffusivity were best adapted to the chips. These beads have a diameter of $2.9\mu m$ and a diffusion constant $D = 0.82 \pm 0.07 \cdot 10^{-13}\, m^2/s$. This diffusion constant had been previously measured in the rectangular microstructured channels, but had not been checked in the new channels, since nothing suggested that it has changed.

The next step was to place the plexiglas device holding electrodes over the chips (see fig 6). The surface of the plexiglas was beforehand cleaned with water to prevent the contamination of the chips with dust. The plexiglas was then placed on the microscope's stage, and the best channel was chosen (the structures had to be well in place with a regular shape and no air bubble should be present). $5mL$ of the beads' solution were placed in one reservoir of this channel. Ideally, the beads should have entered at this point the narrow entry channel by hydraulic pressure, but they often needed to be helped along. $25mL$ of the "Tween solution" were thus added on the same reservoir, and the induced hydraulic pressure was generally sufficient to push the beads inside the channel. $30mL$ of the "Tween solution" were finally put in the opposite reservoir, so that the two electrodes were immerged in the fluid and that the same pressure was exerced on both sides of the channel.

3.3 Observation

The photography on fig 6 shows a view of the whole experimental setup. The electrodes on the plexiglas slide were connected via a switching device controlled by a computer software to two voltage generators of an accuracy of 1 volt which deliver voltages up to several hundred volts. One generator delivered the voltage $A + F$, the other one

$A-F$. During a first time τ one electrode (electrode "α") was put at the $A+F$ potential and the other one (electrode "β") was connected to the ground. Then, the connections were switched, and during another time τ the electrode α was linked to the ground and the electrode β to the $A-F$ potential. The whole cycle was repeated again and again. The value of the electric field being defined as $E = V_\alpha - V_\beta$, the voltage in the channel was thus alternating between $A + F = |U_{AC}| + U_{DC}$ and $F - A = -|U_{AC}| + U_{DC}$, as we wanted it to do. The switching device was not perfect : we were able to measure at most a time of $0,3s$ between the switching off of a voltage and the switching on of the following one. However, the switch period τ which were used were about two orders of magnitude higher than that, so the error compared to the ideal instantaneous switching was negligible.

The motion of the beads in the chips was observed through a binocular microscope. A CCD camera was installed over the microscope, so that it was possible to store videos for analysis. Fig7 shows the size of the area that was observable (about $200\mu m \times 400\mu m$). The observed area was chosen in order to have as many beads as possible without interaction, ideally between 40 and 80. A good compromise between the need of precise data, the best possible statistics, the lifetime of the chip (less than 2 hours) and the limitation of storage place was to film the beads during 4 complete periods of driving ($8\tau \simeq 4min$) by storing 4 frames per second. This was providing enough time to run the experiment for a dozen different sets of voltage parameters.
The chips were lit from beneath with a mercury lamp, and the sensibility of the CCD camera could be adapted to the light in order to have the best possible contrast on the video.

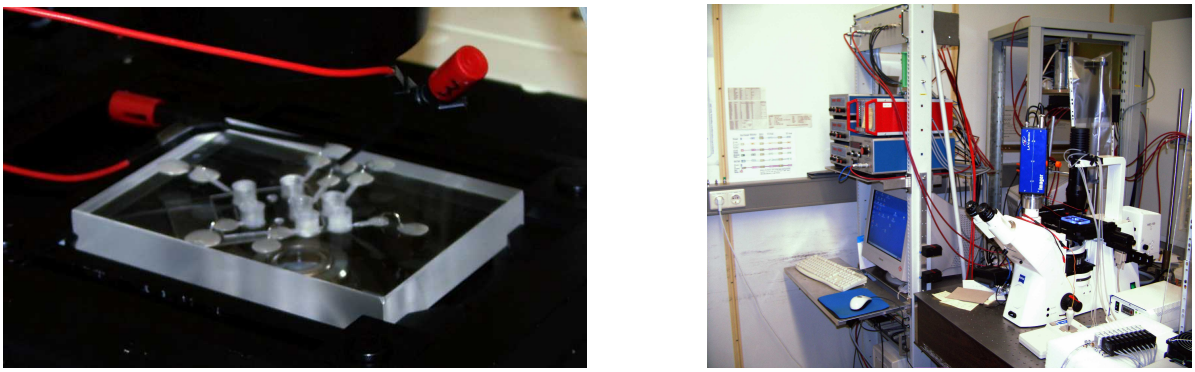

FIG. 6 – The photography on the left shows the plexiglas device placed on the stage of the microscope. The PDMS chip displayed on the previous photography is noticeable under the plexiglas. Crocodile clips connect the electrodes of the plexiglas device to the generators. On the right, an overview of the whole setup.

3.4 Analysis

The range of usable parameters $\{A, F, \tau\}$ was limited by several experimental factors. For example, too high voltages increased annoyingly the magnitude of the EOF flow. Another kind of problem was caused by the elastomeric properties of PDMS : a bead driven by a strong electric force could be forced between two posts, and thus really be held between them and not just pushed against them. Therefore, when the voltage was switched in the other direction, it had to be superior to a certain minimum for the bead to get out of the trap immediately. We used voltages between 5 and 160 volts, a range in which these problems were limited.

Once decided which value of A and F were going to be tested, the switching period τ was chosen high enough to allow the beads to cover more than two spatial length L (see fig 7) along the x-axis, for most of the driving voltage $F \pm A$. In fact, τ had to be at least high enough for all the beads to be trapped at the end of each period. In that way, the whole system was "reset" at the end of each period 2τ, which was statistically advantageous as the effective number of independant beads observed was then the product $N = nP$ where n is the number of beads observed and P the number of periods during which they are followed. Typically, switching period of 25 or $30s$ were used, and the beads were observed during 4 periods.

As the $2.9\mu m$ beads that were most frequently used were not fluorescent, the analysis

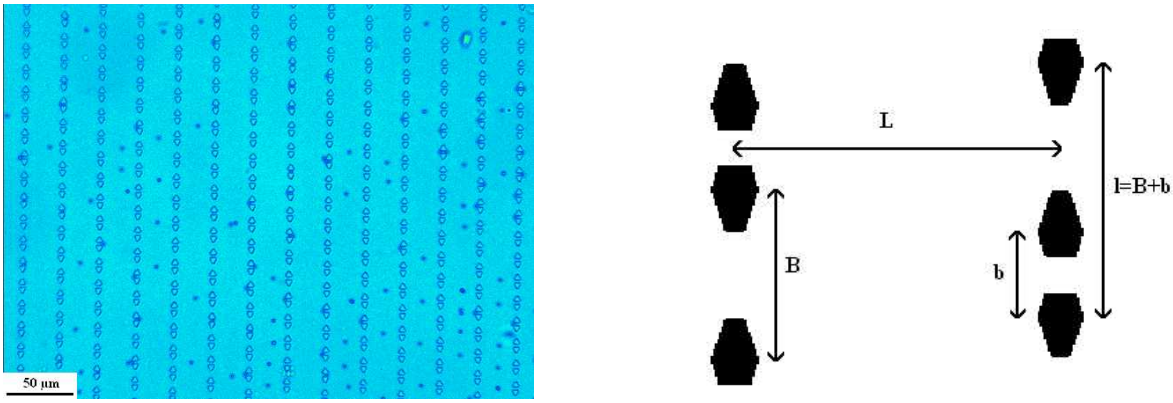

FIG. 7 – On the left, an extract of a video taken with the CCD camera. On this image, a new time period has begun some seconds before : the beads have just left the traps and are moving to the left. Note the fact that the beads are roughly aligned. On the left, a schema presenting the different length scale of triangular chips. L is the distance from row to row, l is the periodic length in the y-direction. The latter can be divided into a "trap zone" of length b and a "free zone" of length B. The separation between these two zones coreesponds to the point where the electric field separates (see fig3), a point that we have considered to be facing the peaks of the posts.

of the beads' motion was difficult to handle with an image treatment software. Moreover, some other problems such as beads sticking to the PDMS surface or sticking to each other (thus creating artificial bigger beads with a different mobility) made the option of the image treatment software not entirely reliable. The analysis was then done "by

hand", by systematically measuring the length coverred by each bead during each period 2τ, which was almost always a manyfold of the length L since the beads were almost all (more than 95% with the set of parameters we used) trapped before the end of each period. The mean velocity v was computed by averaging all these length over the N effective beads and dividing this average length by the time 2τ. A statistical error was defined as $\frac{\Delta v}{\sqrt{N}}$, where Δv is the usual standard deviation and $\sqrt{N}$ an additionnal factor added to compensate the huge values of Δv caused by the fact that the averaging is done over a discrete variable which can only takes some values. The mobility of the beads was checked each time in both directions by measuring the time t needed for typically a dozen beads to cover the distance $2L$ between one trap and the corresponding opposing trap, then using $\mu =< \frac{2L}{Et} >$.

4 Results

In this section we present the most complete and interesting results which have been obtained during the training period. Some other results are presented in the appendix.

4.1 Results in $E2$ channels

The behaviour of the $2.9\mu m$ beads in the $E2$ channels[6] is presented fig 8. The passage through the origin with a negative slope, which is the basic signature of ANM, is obvious both in the simulation and in the experimental results. Furthermore, the maximum velocity in the ANM direction is about $0.075\mu m/s$, which means that the ANM effect has been improved by at least a factor 7 compared to the first experiments with the rectangular geometry !

On this particular sequence of measurements, we work with the parameters $A = 80V$ and $\tau = 30s$. The mobility of the beads was not constant in time (see section 5.2), varying between $0.11\mu m/Vs$ and $0.16\mu m/Vs$ during the 2 hours needed to carry out the measurements. However, the simulation, run with a constant mobility $\mu = 0.13\mu m/Vs$, is in excellent agreement with the experimental data.

The interpretation of the shape of the simulation curve is here rather easy to make. Let us introduce the parameter $\lambda = \frac{\mu E \tau}{L}$. λ corresponds to the number of distance L a bead could potentially cover in the x-direction during the time τ and driven by an electric field E in case it was not stopped by the posts. Let us study the $U_{DC} = F \geq 0$ part of the graph. In this part, the beads are alternatively driven to the left by a voltage $E_{weak} = A - F$ and to the right by a voltage $E_{strong} = A + F$.

When $\lambda_{weak} \geq 3$ (F between 0 and 59 volts), the value of E_{weak} is sufficient for the beads to cover a distance superior to $3L$ to the left. Most of the beads get caught in the first trap and come back to their initial place at the end of the period 2τ (see fig 9-B), but some of them avoid the first trap by diffusing in the y-direction (fig 9-A). As E_{weak} get smaller ($F = U_{DC}$ increases), the beads have more time to diffuse, which give them more chance to avoid the first trap. Consequently, the mean length covered by a bead

[6] the channels have been named after their place on the wafer, "$E2$" thus corresponds to the second group of four channels in the East direction of the wafer

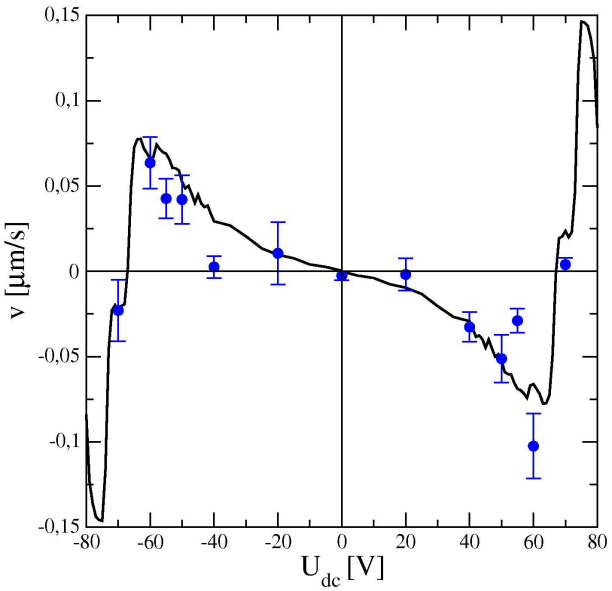

FIG. 8 – Velocity response of $2.9\mu m$ beads in a $E2$ channel. Here, an amplitude $A = 80V$ and a switching time $\tau = 30s$ were used. Dots with error bars : experimental data, the average is done for around 60 beads followed during 4 driving periods. Solid curve : results of a simulation run for 10 beads during X periods, with mobility parameter $\mu = 0.13\mu m/Vs$.Velocity response of $2.9\mu m$ beads in a $E2$ channel. Here, an amplitude $A = 80V$ and a switching time $\tau = 30s$ were used. Dots with error bars : experimental data, the average is done for around 60 beads followed during 4 driving periods. Solid curve : results of a simulation run for 10 beads during 500 periods, with mobility parameter $\mu = 0.13\mu m/Vs$.

to the left during the total period 2τ is rising and so is $|v|$.

For $2 \leq \lambda_{weak} \leq 3$ (F between 59 and 66 volts), there is a transitory regime. As λ_{weak} decreases, the beads can not any more cover the length $3L$ to the left as in fig 9-A and the percentage of "ANM-beads" is rapidly decreasing. As λ_{weak} approaches 2, some of the beads begin to avoid their initial trap on their way back to the right, because of the diffusion that occured during the weak half-period, and thus contribute for a positive mean velocity.

The small plateau between $F = 66$ and $F = 73$ exactly corresponds to $1 \leq \lambda_{weak} \leq 2$. The motion which contributes to the non-zero value of v is the one presented fig 9-C. It is interesting to note that the same kind of plateau was also present in the initial experiment with the rectangular post (see fig 2).

Finally, when λ_{weak} crosses the value 1, the beads do not have any more the possibility to go beyond the first row on the left before the switching. Therefore, they do not have the possibility to have an effective motion to the left during one period. The contributing motion becomes the one presented fig 9-D, which is more or less probable given the values of $F \pm A$. v goes throught a maximum before falling to zero : for $\lambda_{weak} \leq 0$, the electric field is always directed to the right, and consequently, once a bead is trapped, it remains trapped forever.

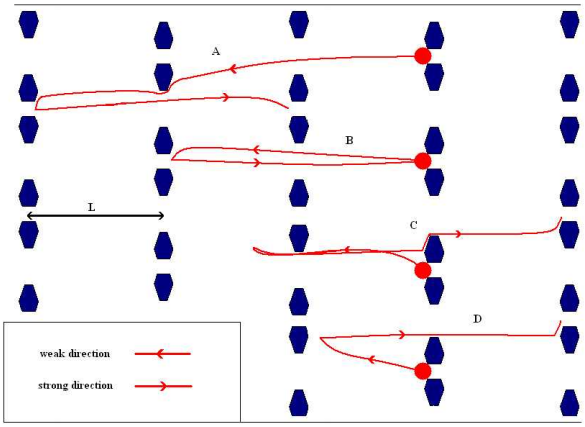

FIG. 9 – Some of the numerous behaviours of the beads. In A/ $\lambda_{weak} \geq 3$: if the bead avoids the first trap it can reach the following one during the "weak" half-period, and then go back to the right during the "strong" half period. As the field is stronger in that direction, the bead is this time less likely to avoid the first trap. B/ Experimentally, more than 90% of the beads are just going back and forth between one trap and its opposite one, provided $\lambda_{weak} \geq 2$. C/ $1 \leq \lambda_{weak} \leq 2$: some of the beads present a normal response, their mean motion having the same sign as the mean force. D/ When $\lambda_{weak} \leq 1$, a positive response can also occur.

4.2 Results in $W2$ channels

The behaviour of the same $2.9\mu m$ beads in the $W2$ channels is presented in fig 10. We were able to make measurements in slightly different conditions that provide results for two different mobilities (see discussion in section 5.2). The general shape of the curves is roughtly identical to that of the curves in the $E2$ channel and once again, the possibility to obtain ANM in microstructured channel is confirmed. We observe here an improvement of a factor 9 compared to the initial rectangular geometry.

The agreement between the simulations and the experimental results, if not as good as in the $E2$ channel, is still more than acceptable. The large error bars are mainly due to a lack of data : we were able in these two experiments to follow only around 30 beads, *ie* only half of the number of beads followed in the experiment in the $E2$ channel presented in the previous section.

The importance of the value of the beads' mobility is emphasized by the difference of the shape of the two simulation curves fig 10. The curve on the right, corresponding to the greatest mobility, has a very shallow slope at the origine, compared to the other one. In fact, we even have $|v_{fast}(F)| \leq |v_{slow}(F)|$ for each value of F. The interpretation is straightforward : as the beads are moving faster, they have less time to diffuse, and thus a lower percentage are avoiding the traps.

An other remarkable feature displayed by these graphs is the fact that the normal response for $|F| \geq 65$ or $70V$ is more important than in the $E2$ channel. This is explained by the fact that the mean behaviour of the beads is quite different in the two channels, because of a tiny difference in the geometry of their posts (see section 5.1).

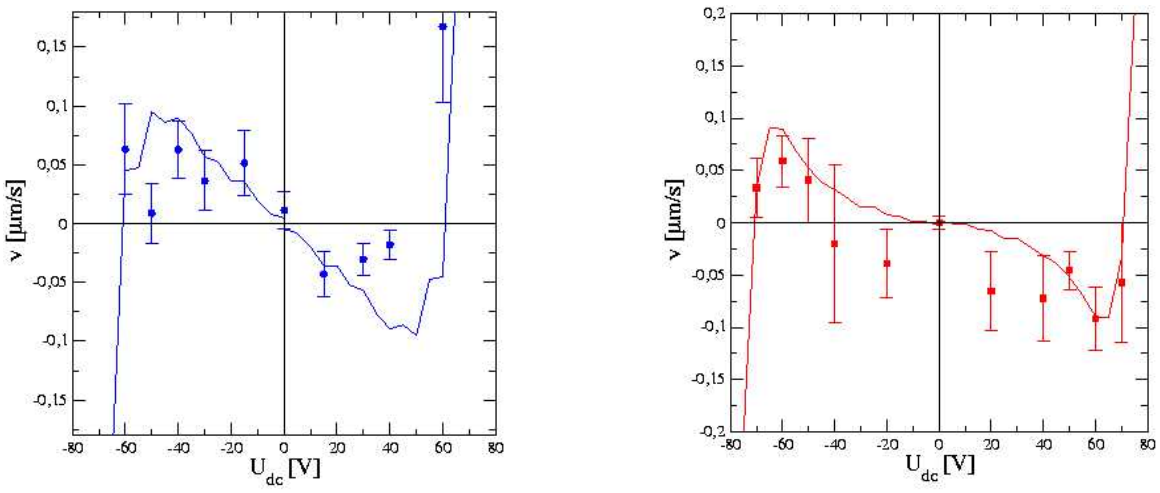

FIG. 10 – Velocity responses of $2.9\mu m$ beads in two $W2$ channels. In both cases, an amplitude $A = 80V$ and a switching time $\tau = 30s$ were used. On the left, the mean mobility of the beads was $\mu_{slow} = 0,11\mu m/s$; on the right it was $\mu_{fast} = 0,23\mu m/s$. Dots with error bars : experimental data, the average is done in both case for around 30 beads followed during 4 driving periods. Solid curves : results of the simulations run for 10 beads during 500 periods.

5 Discussion

5.1 "Pure ANM" versus "deterministic path"

The $E2$ and $W2$ chips, seen from the optical microscope, falsely seem to be not different : they are both chips with "triangular" shaped posts. However, it was obvious in the experiments that the beads do not behave in the same way in the two kind of channel. In both chips, around 90% of the beads were doing the back and forth motion of fig 9-B, but :

• in $E2$, the rest of the beads were able to avoid one or two traps when moving in the weak-field direction, which permitted them to effectively cover a distance L or $2L$ in the ANM direction during one period 2τ (provided they were immediately trapped in the strong-direction). The mechanism governing this kind of motion is the only one which has been presented until then (see section 1 and 4.1), we called it the "pure ANM" mechanism.

• in $W2$, the situation was different. The beads were indeed able to avoid much more traps : on the video we could see them slaloming between the post and effectively coverring distances of $5L$ to $10L$ in one period, when for the same voltage and an equivalent mobility they could not do more than $2L$ in an $E2$ channel. This "slalom wandering" was totally unexpected, and the SEM images on fig 11 give us the reason of its existence : it seems that by accident of production, the "free zone" is a bit larger in $W2$ channels, whereas the "trap zone" is a bit smaller. And this difference of $200nm$ is not without consequence.

Let's imagine the motion of a bead starting from a trap and moving to the right in

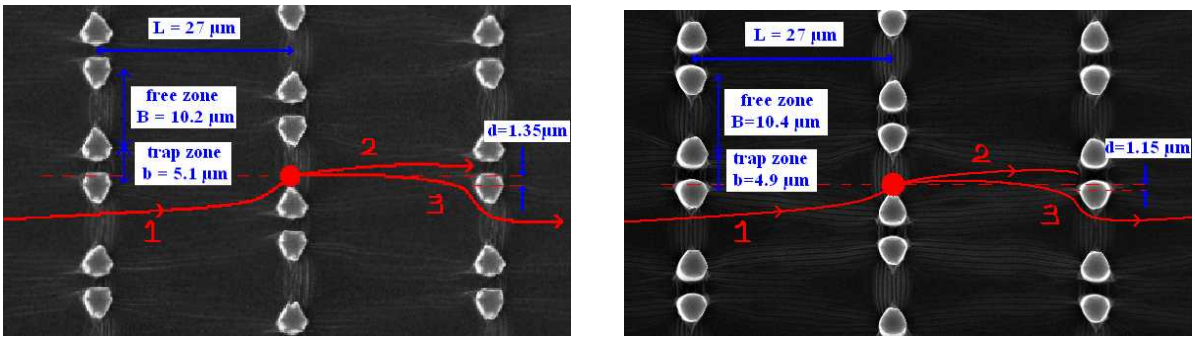

FIG. 11 – Scan Electron Microscopy images which allow us to measure precisely different lengths in the channels. In the $E2$ channel on the left, we found $L = 27 \pm 0.1\mu m$, $B = 10.2 \pm 0.1\mu m$ and $b = 5.1 \pm 0.1\mu m$. In the $W2$ channel on the right, we found $L = 27 \pm 0.1\mu m$, $B = 10.4 \pm 0.1\mu m$ and $b = 4.9 \pm 0.1\mu m$. The length d corresponds to the minimum length a bead had to cover along the y-axis in order to avoid its n^{th} trap just after it has avoided its $(n-1)^{th}$ trap $(n \geq 2)$.

a given channel and driven by a given voltage E. In order to avoid the first trap, our bead has to get out of the "trap zone" before reaching the opposite posts, *ie* to diffuse at least over a length $b/2$ along the y-axis while moving over a distance a little shorter than $2L$ along the x-axis(see fig 11). Suppose that our bead avoid this first trap (the trajectory of our bead is so far represented by the trajectories marked with a "1" on the SEM images). Then, our bead could either get caught in the following trap (trajectories "2") or it could also avoid this second trap (trajectories "3"). In order to avoid this second trap, our bead has to diffuse over a minimum length d along the y-axis while moving over a distance near to L along the x-axis. The shorter d is, the more chance there is to avoid the second trap. The same scenario then hold for the following traps. The fact that $d(E2)$ is superior to $d(W2)$ implies that it is more probable for a bead to avoid the second and following traps (provided the first one has been avoided) in a $W2$ channel than in a $E2$ one. In other words, the "slalom wandering" will occur more often in the $W2$ channel. This is more than obvious on the histograms presented fig 12.

The channels can be further characterized by another criterion. The probability to avoid the first trap must be a decreasing function of

$$\frac{\mu E b^2}{8LD}$$

which is the ratio of the characteristic times $\frac{(b/2)^2}{D}$ needed to diffuse along a distance $b/2$ and the characteristic time $\frac{2L}{\mu E}$ needed to cover the distance from the initial point to the first trap. In the same way, the probability to avoid the n^{th} trap once the $(n-1)^{th}$ $(n \geq 2)$ has been avoided must be a decreasing function of

$$\frac{\mu E d^2}{LD}.$$

Now, it appears that we have $d(E2) = 1.35\mu m \leq b(E2)/2\sqrt{2} = 1.80\mu m$ and $d(W2) = 1.15\mu m \leq b(W2)/2\sqrt{2} = 1.73\mu m$. These inegalities imply that in both chan-

nels the beads have more chance to avoid the second and following traps than they have to avoid the first one. This criterion is verified experimentally : it is obvious in the histograms of fig 12 that there is systematically the isolated peak of the beads that do not avoid the first trap in either direction and thus had a zero motion over the whole period. Besides this isolated peak, the distributions are rather flat (moreover in the $W2$ channels, thanks to the "slalom wandering"), or slowly decreasing with the number of length L covered during one period.

Now, the question is to know whether one of the two mechanisms is better than the other one as regards to the ANM effect. The advantage of the "slalom wandering" is that a bead can go very far (once it has avoided the first trap) by slaloming between the posts. But the "slalom wandering" can occur both in the weak, ANM, direction and in the strong, normal, direction. Of course the probability to avoid the first trap in a certain direction depends on the value of the electric field in this direction, and it is less likely for stronger field. Nonetheless, once a bead has avoided the first trap in the strong direction, it can cover larger distances than in the weak direction, because it moves faster (see the distributions for the $W2$-slow channel at $|F| = 40$ and $50V$). As the beads gave the impression to ignore the microstructures while slaloming, we also called this mechanism "deterministic path". All in all, the improvement of the ANM effect is greater in the $W2$ channel than in the $E2$ one (improvement by a factor 9 versus improvement by a factor 7). The problem is that the $W2$ channel were built "by accident", and that the difference of $200nm$ between its structure and the $E2$ structure was originally in the range of the errors accepted in the fabrication process of the SU-8 molds. So the "slalom" chips might not be that easy to create or re-create.

5.2 Mobility

The mobility of the $2.9\mu m$ beads was found to be rather unpredictable. In all the chips we used (built from the same $W2$ and $E2$ molds), we measured several mobilities between 0.10 and $0.40\mu m/Vs$. Althought some of the factors which influenced the value of the mobility were identified and controlled, most of them were only suspected and difficult to control. Among other, the diameter of the reservoirs of the plexiglas device, the temperature of PDMS curing, the time of exposure to the oxygen plasma, the room temperature... controlled more or less directly the pressure inside the channels or the PDMS surface properties, and thus had an influence on the EOF, therefore on the beads' mobility.

The computation of the mobilities we made throughout the analysis of the video sequences allow us to discuss two of these factors. In fig 13, we display the mobilities we found in two different series of experiments, giving separately the values of the mobility in the weak direction and in the strong direction. The mobility was almost always a bit stronger in the weak direction. There is a saturation of the system at higher electric field : the EOF increases with the electric field faster than electrophoresis.

On one similar experimental device, increase of two unity of pH between the time when the reservoirs were filled and the end of the experimental work (around 1 hour) were measured with pH indicator paper. The change in pH could be explain by the evaporation of water which would imply an increase of the ions concentrations and shift

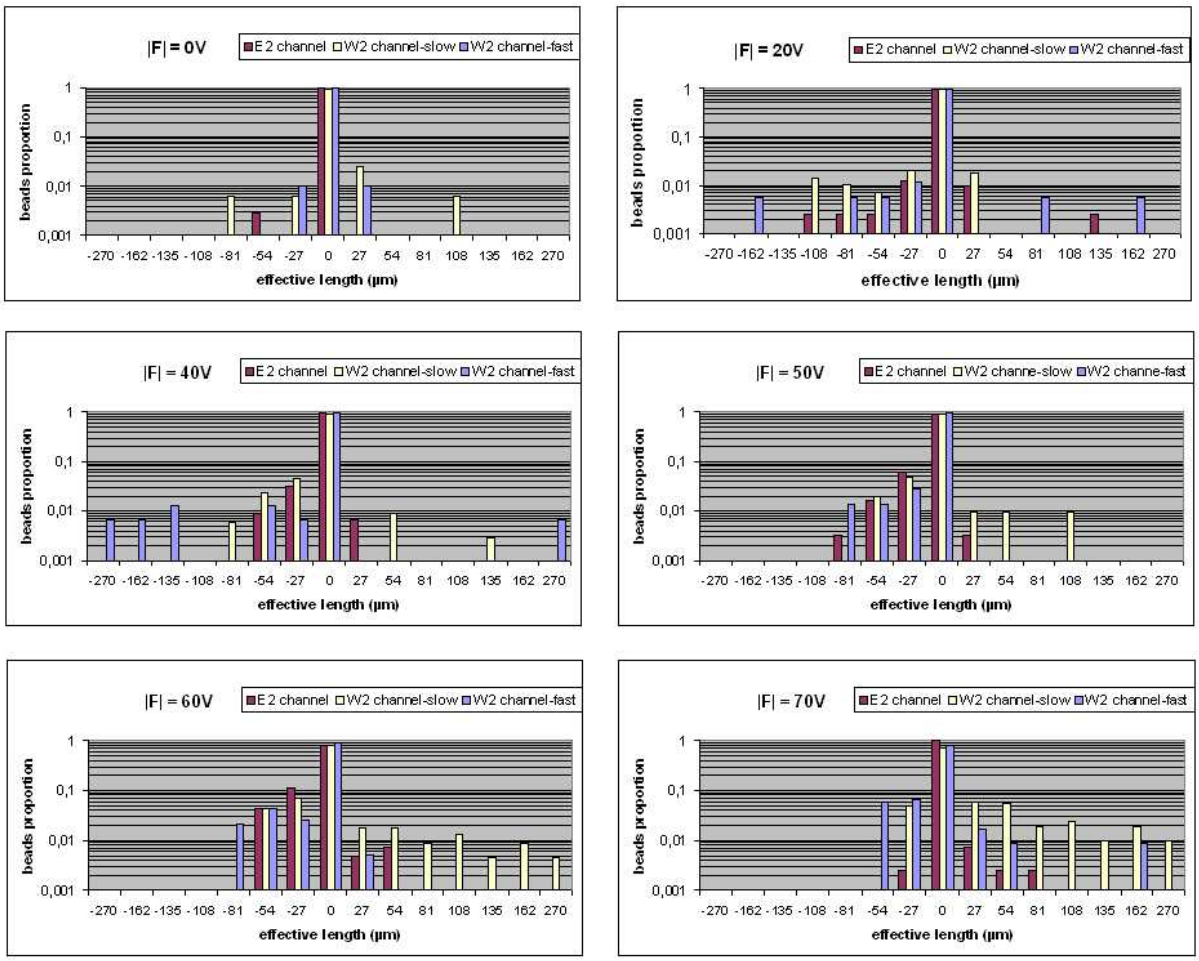

FIG. 12 – Several histograms presenting the experimental beads distributions for different values of $|F|$ in the 3 experiments presented section 4. The "effective length" on the abscisse corresponds to the length coverred by the beads during one period 2τ. Positive values of this effective length correspond to normal response and negative values correspond to ANM response. For a given $|F|$, the distributions have been computed in each case by taking into account the motion of all the beads during each of the 4 periods of observation stored for $F = |F|$ and $F = -|F|$. Note that there is almost always more than 90% of the beads that are just doing a forth and back between two traps. Logarithmic scale is used for the ordinates in order to well appreciate the rest of the distributions.

all the chemical equilibriums. It could also be implied by the effect of the use of electric fields which could change the surfaace properties of PDMS. The change of pH could thus change the amplitude of the EOF. That is why, when we found that the mean mobility of the beads was decreasing linearly with time (see fig 13) we ended up to suspect an increase in pH.

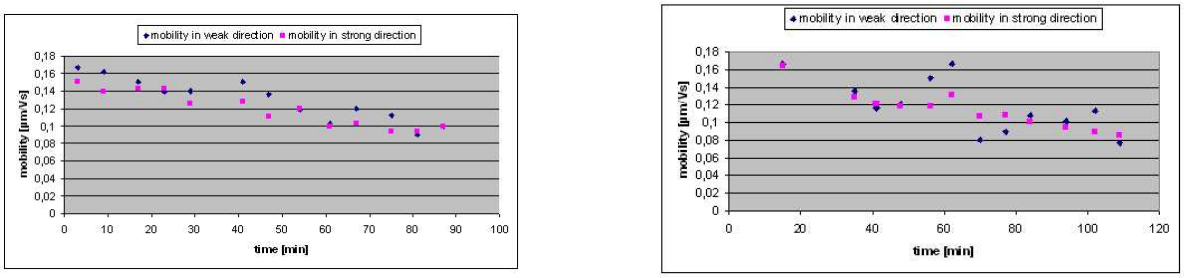

FIG. 13 – The mobility seems to decrease more or less linearly with time during the experiments. This is certainly due to the evaporation of the buffer in the reservoirs which tends to increased the pH in the channels. On the left, time dependance of the mobility (measured in each sequence in the strong and weak direction) with time in the $E2$ experiment. The reservoirs were refilled at time 39, 64 and 83. On the right, time evolution of mobility in the $W2$-slow experiment. The reservoirs were here refilled at time 28, 52, 72 and 96. The fact that the mobility increases a bit after each refilling confirms the pH hypothesis. Note also that the mobility in the strong direction is always a bit inferior to the mobility in the weak direction : the law which links the free velocity to the electric field is not exactly linear, but slightly concave.

5.3 Practical interest of ANM

The work presented in this report is above all giving the proof that ANM exists outside the quantum world. But the ANM effect might also have a lot of practical interest. It has been shown [6] that the ANM effect could be used for example as an alternative to electrophoresis to separate two kind of beads, one of which would move in the ANM direction whereas the other one would moves in the normal direction (see also the section 9.2 in appendix for this subject).

5.4 More subjects of discussion

All the experimental choices could be subject to discussion, from the time and temperature used to cure PDMS to the time and intensity of the glow discharge during the exposure of the microstructure to the oxygen plasma, via the buffer chosen to coat the chips. But the only remaining fact we wanted to comment on is the fact that less than 1/4 of the 32 mold on the wafer were usable. The reason is that the SU-8 molds are adapted for structres of characteristic length down to around $10\mu m$. However, the posts we needed to built had to be 3 times smaller. The Scan Electron Microscopy image

presented fig 14 shows how difficult it is to build microstructures of this size.

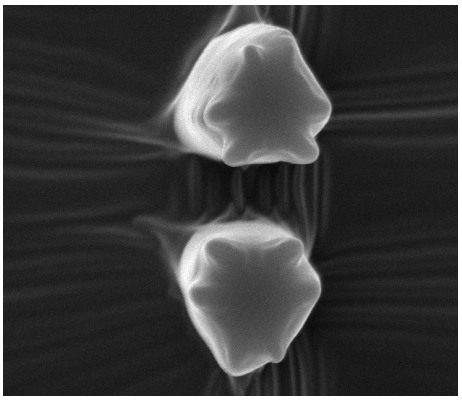

FIG. 14 – SEM image providing a very close view of two $E2$ posts. The structure on the edges of the posts are the effects of the interference and diffraction of the UV light caused by the edges of the chromium mask during the SU-8 exposure to UV light. The posts we tried to built were so small that some of their characteristic length became comparable with the wavelength of the UV light ($365nm$).

6 Conclusion

The first noticeable matter is that the existence of ANM in microfluidic device is experimentally confirmed, which is important considering the very few experimental proof that existed until then. In several of the new geometrically modified microstructured channels, the ANM response has been improved by a factor 7 in comparison with the response of the first designed "rectangular" microstructures. In one of these new channels the beads had a motion following a particular mechanism that we called "slalom wandering". Thanks to this mechanism, the ANM response has been improved by a factor 9 in this particular channel.

This work has been successful in the sense that we now know for sure that the geometry of the microstructures can be modified to noticeably enhance the ANM response. In the next generation of chips, it could for example be interesting to try to find geometries to the "slalom wandering mechanism" in order to further amplify the ANM response. But the amplification that could be created this way should not be very important, and above all the chips that would be designed this way would work only with specific kind of beads or particles. The goal is now to see whether the chips work for other kind of beads, and to study the range of response these different beads offer. Another idea, which is currently developped in order to further improve the ANM response, is to try to enhance the diffusion along the y-axis. There is still much to be done before ANM could be used for direct biological applications.

7 Acknowledgements

I would like to thank warmly all the people of the Departement of Biophysics of the University of Bielefeld for their welcome, and among them especially : Jan Regtmeier, Stefan Gerkens, Dominic Greif, Alexandra Ros. Thanks to Stefan, for introducing me at the beginning of my stay in Bielefeld to the world of experimental biophysics and to the chemical secrets of PDMS. Thanks to Jan for his helpful advices, for our discussion upon every little aspects of the experiment and for his critical reading of the first version of this report. All the mispellings, imprecisions or errors that remain are totally mine.

8 References

[1] T.J.Banys, I.V.Parshelyunas, Y.K.Pozhela, *Sov. Phys. Semicond.* **5**, 1727 (1972)
Absolute negative resistance of Gallium-Arsenide in a strong microwave field

[2] B.J.Keay *et al.*, *Physical Review Letters* **75**, 4098 (1995)
Photon-Assisted Electric Field Domains and Multiphoton-Assisted Tunneling in Semiconductor Superlattices

[3] P.Reimann, R.Kawai, C.Van der Broeck, P.Hänggi, Europhys. Lett. **45**, 545 (1999)
Coupled Brownian motors : Anomalous hysteresis and zero-bias negative conductance

[4] R.Eichhorn, P.Reimann, P.Hänggi, Physical Review E66, 066132 (2002)
Paradoxical motion of a single Brownian particle : Absolute negative mobility

[5] R.Eichhorn, P.Reimann, *Acta Physica Polonica B* Vol.37 (2006)
Analytic theory of absolute negative mobility in a microfluidic device

[6] A.Ros, R. Eichhorn, J. Regtmeier, *et al.*, Nature, **436**, 928 (2005)
Absolute Negative Particule Mobility

[7] W.Hellmich, J.Regtmeier, T.Duong *et al.*, Langmuir, 21, 7551-7557 (2005)
Poly(oxyethylene) Based Surface Coatings for Poly(dimethylsiloxane) Microchannels

9 Appendix

We present in this section some other results, which well illustrate the range of what can be achieved with our microstructured channels as well as the practical difficulties we encountered when using them.

9.1 In $E2$ channel

In fig 15 we presents results obtained in a $E2$ channel by using an amplitude $A = 50$ and a switching time $\tau = 30s$. The mean mobility of the $2.9\mu m$ beads was found to be $\mu = 0.28\mu m/Vs$. The greatest velocity in the ANM direction is still around 7 times higher than the reference of the "rectangular" chips. In this experiment, we were able to take only 4 videosequence because for some reason the adherence between the PDMS and the plexiglas was not perfect, and some fluid coming from the reservoirs leaked between the PDMS and the plexiglas. A pressure gradient appeared in the channel which created a small drift in the left direction. This drift could explain the difference between the experimental data and the simulation. The point corresponding to $F = -30V$ is the last that was measured, just before the drift was noticed.

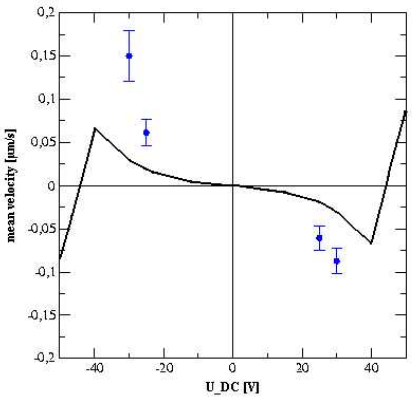

FIG. 15 – Velocity response of $2.9\mu m$ beads in a $E2$ channel. Here, $A = 50V$ and $\tau = 30s$. Dots with error bars : experimental data, the average is done for around 70 beads followed during 4 driving periods. Solid curve : results of a simulation run for 10 beads during 500 periods, with mobility parameter $\mu = 0.28\mu m/Vs$.

9.2 In $W2$ channel

The fig 16 presents results obtained in $W2$ channel. In this particular experience, two kind of beads (with a diameter of $2.9\mu m$ and $1.9\mu m$) were placed in the chip. In order to avoid any interaction between the beads, we put only $3mL$ of each of the two Tween solution containing the beads in the first reservoir instead of the usual $5mL$. The concentration of each kind of bead was therefore small : we were able to follow only some

30 beads of each kind during 4 periods. We worked with parameters $A = 80$, $\tau = 30s$ and a mean mobility of $0.28\mu m/Vs$ was measured, the same (by coïncidence) for the two kind of beads.

With this experiment, we wanted to prove that it was possible to separate two kind of micro-objects in our microstructured channel. It worked perfectly because the $1.9\mu m$ beads were small enough to go throught the small gaps, and thus had almost all ("almost" because some of them were stopped by irregularly smaller small traps or sticked to the PDMS surface) a free-deterministic motion, whereas the $2.9\mu m$ beads were stopped and trapped in the small gaps. As a consequence, when the $2.9\mu m$ beads were having an ANM motion, the $1.9\mu m$ ones were having mean velocity 100 times higher in the "normal" direction.

Of course, in this case, the two kind of beads were separated mainly because one of them was on the average moving 100 times faster than the other one and not because they were moving in different directions. Ideally, we should have found two different kind of beads, both of them being stopped by the traps, such that for one set of voltage parameter one of them would have presented an ANM response and the other one a normal response. This had been done in the initial experiments with the rectangular posts, where the two kinds of beads were moving in opposite direction with velocity modulus of the same magnitude. However, we did not have the time or the luck to manage to do this kind of observation.

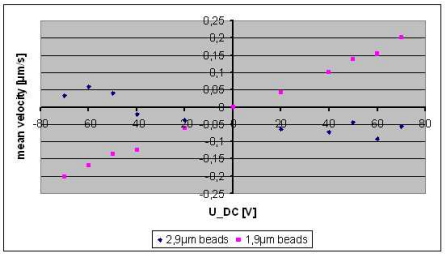

FIG. 16 – Velocity response of $2.9\mu m$ and $1.9\mu m$ beads measured in the same $W2$ channel. Both kind of beads had a mean mobility of $0.28\mu m/Vs$. The $2.9\mu m$ beads present an ANM response (the data corresponding to these beads has already been presented in section 4.2). The $1.9\mu m$ beads were so small that they could go throught the small gaps : they acted as if the microstructures were not there. This explains the linear response which corresponds to $v = \mu F$. Here, the velocity of the $1.9\mu m$ beads has has been divided by 100.

9.3 In $N1$ channel

On the fig 17, we present results obtained in a $N1$ "square" channel. We had a lot of troubles with these channels, mainly because many posts were not height enough to stick to the bottom of the channel. This was certainly caused by the presence of thin layer of SU-8 remaining at the place of the "negative posts" on the wafer. The small vertical gaps that were thus created between the posts and the bottom of the PDMS channel were large enough to let the beads go through them (thus rendering the system of trap

of the microstructure inefficient). This particularity also rendered the phenomenon of "elastic traps" described in section 3.4 much stronger. That is why we were able to record only 4 sequence on this experiment : at the beginning we measured the motions of around 50 beads and 20 min later, only 5 of these initial beads were free to move.

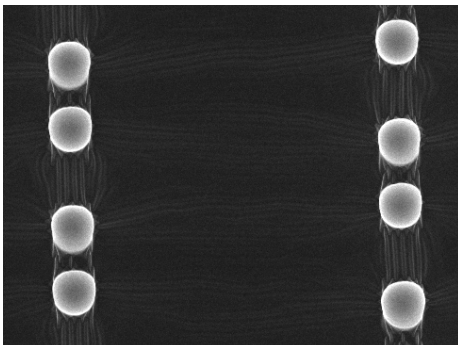

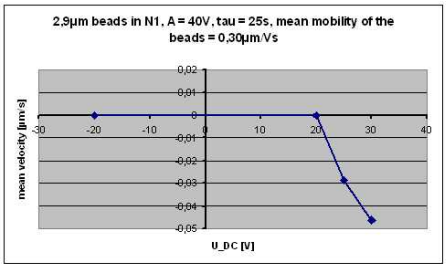

FIG. 17 – On the Left : Scanning Electron Microscope image of a $N1$ channel. The $N1$ channels should have been made of square posts, but we ended with a mold made of more octogonal-shaped posts. The distance from row to row is $L = 23\mu m$. On the right : an exemple of results obtained in a $N1$ channel. On this particular experiment, $A = 40$ and $\tau = 25s$. The mobility of the $2.9\mu m$ beads was $mu = 0.30\mu m/Vs$ and the average was done for around 40 beads followed during 4 periods.